Dynamics of cortical local connectivity during sleep/wake states and the homeostatic process

Takehiro Miyazaki[1,#], Takeshi Kanda[1,#,†], Natsuko Tsujino[1], Ryo Ishii[1], Daiki Nakatsuka[1], Mariko Kizuka[1], Yasuhiro Kasagi[1], Hideitsu Hino[3], and Masashi Yanagisawa[1, 2, 4, 5]

[1]International Institute for Integrative Sleep Medicine, University of Tsukuba, Ibaraki 305-8575, Japan
[2]Departments of Molecular Genetics, University of Texas Southwestern Medical Center, Dallas, TX 75390-9050, USA.
[3]The Institute of Statistical Mathematics, Tokyo 190-8562, Japan
[4]Life Science Center for Survival Dynamics (TARA), University of Tsukuba, Ibaraki 305-8575, Japan.
[5]R&D Center for Frontiers of Mirai in Policy and Technology (F-MIRAI), University of Tsukuba, Ibaraki 305-8575, Japan.

† Address corresponding to Takeshi Kanda,
International Institute for Integrative Sleep Medicine, University of Tsukuba, Ibaraki 305-8575, Japan
E-mail, kanda.takeshi.fu@u.tsukuba.ac.jp
Tel, +81-29-853-3301
Fax, +81-29-853-5735

# These authors contributed equally to this work.

Abstract

Sleep exerts modulatory effects on the cerebral cortex. Whether sleep modulates local connectivity in the cortex or only individual neural activity, however, is poorly understood. Here we investigated functional connectivity, that is, covarying activity between neurons, during spontaneous sleep-wake states and during and after sleep deprivation using calcium imaging of identified excitatory/inhibitory neurons in the motor cortex. Functional connectivity was estimated with a statistical learning approach glasso and quantified by "the probability of establishing connectivity (sparse/dense)" and "the strength of the established connectivity (weak/strong)." Local cortical connectivity was sparse in non-rapid eye movement (NREM) sleep and dense in REM sleep, which was similar in both excitatory and inhibitory neurons. The overall mean strength of the connectivity did not differ largely across spontaneous sleep–wake states. Sleep deprivation induced strong excitatory/inhibitory and dense inhibitory, but not excitatory, connectivity. Subsequent NREM sleep after sleep deprivation exhibited weak excitatory/inhibitory, sparse excitatory, and dense inhibitory connectivity. These findings indicate that sleep–wake states modulate local cortical connectivity, and the modulation is large and compensatory for stability of local circuits during the homeostatic control of sleep, which contributes to plastic changes in neural information flow.

Keywords: calcium imaging, graphical model, motor cortex, neural connectivity, sleep

Introduction

Animals spontaneously transition between sleep and wakefulness, which is regulated by and functionally required for the nervous system. Although sleep contributes to several brain functions, including learning and memory, the phenomenon of sleep itself is yet unexplained. In mammals, characteristic patterns emerge in the electroencephalogram (EEG) during sleep and are associated with several brain functions, indicating that sleep supports brain functions by modulating cortical network dynamics. The electrophysiological cortical network activity is distinct between the two sleep states: rapid eye movement (REM) sleep and non-rapid eye movement (NREM). In NREM sleep, slow oscillatory activities are observed in the cortex from the single cell level to the population level (Vyazovskiy and Harris 2013), of which slow-wave activity (SWA, 2–4 Hz) in EEG is a hallmark of NREM sleep. In REM sleep, in contrast, rapid cortical activity is observed, similar to that observed during wakefulness. NREM and REM sleep differentially affect global cortical networks: functional magnetic resonance imaging (fMRI) reveals decreased functional connectivity between cortices during NREM sleep and increased functional connectivity during REM sleep (Horovitz et al. 2009; Koike et al. 2011; Sämann et al. 2011; Spoormaker et al. 2012; Wu et al. 2012; Chow et al. 2013; Picchioni et al. 2013). Not only large-scale functional connectivity between cortices, but also local cortical network dynamics are regulated by sleep and are thought to underlie brain functions (Siclari and Tononi 2017). For example, SWA appears locally in NREM sleep and is correlated with motor learning performance (Huber et al. 2004, 2006). Local cortical network activity during sleep, however, is not well explored. To elucidate the local cortical network dynamics during sleep, here we focused on the superficial layer of the motor cortex, which plays a pivotal role in motor learning (Sanes and Donoghue 2000; Kawai et al. 2015). The motor cortex exhibits motor learning-related neural ensembles (Peters et al. 2017) that are recalled during post-task NREM sleep (Gulati et al. 2014; Yang et al. 2014; Ramanathan et al. 2015) and contribute to memory consolidation (Gulati et al. 2017). Here we optically dissected neural activity in the motor cortex of spontaneously sleeping/waking and sleep-deprived mice under "task-free" natural conditions using two-photon calcium imaging. We evaluated functional connectivity, i.e., covarying activity between a pair of neurons. The dynamics of local cortical networks was explored by analyzing the imaging data based on sparse Gaussian graphical models (GGM) that have been used to model genetic networks (Kishino and Waddell 2000; Toh and Horimoto 2002; Dobra et al. 2004) and global neural networks in fMRI studies (Rosa et al. 2015). Glasso (graphical least absolute shrinkage and selection operator) is a widely used algorithm for structural learning of undirected GGM, which, in our data, allows for estimation of functional connectivity between neurons in local cortical networks.

Materials and Methods

Animals

All experimental procedures and protocols were approved by the Institutional Animal Care and Use Committee of the University of Tsukuba. We used Vgat-tdTomato mice generated by crossing Vgat-ires-Cre mice (*Slc32a1*$^{tm2(cre)Lowl}$/J, Jackson Laboratory stock number: 016962) (Vong et al. 2011) with Ai9 tdTomato reporter mice (B6.Cg-*Gt(ROSA)26Sor*$^{tm9(CAG\text{-}tdTomato)Hze}$/J, Jackson Laboratory stock number: 007909) (Madisen et al. 2010). All Vgat-tdTomato mice were maintained on a C57BL/6 background and genotyped by polymerase chain reaction of tail tissue DNA. Mice were fed *ad libitum* and maintained in a temperature- (22°C) and humidity- controlled room under a strict 12-h light-dark cycle (lights on 9:00 a.m. to 9:00 p.m.).

Surgery

Adult mice (9–13 months of age, 2 males and 7 females) were prepared for chronic high-resolution imaging (Mostany and Portera-Cailliau 2008; Holtmaat et al. 2009). Surgery was performed with mice under 2% isoflurane anesthesia. The head hair was removed with depilatory cream (Epilat, Kracie), and the head skin disinfected with an povidone iodine solution (J-IODE Solution, Johnson & Johnson). After incising the skin along the midline and removing the soft tissues above the skull, a small craniotomy (1.5–2.5 mm diameter) was made over the left primary motor cortex, approximately 1.5 mm anterior and 1.5 mm lateral from bregma. Adeno-associated virus (AAV) vectors encoding a calcium indicator, GCaMP6s (Chen et al. 2013) (rAAV-hSyn-GCaMP6s-WPRE, 4.0×10^{13} genomic copies/μl, serotype 2/9, UPenn Vector Core), were injected into 2–3 sites at a depth of 300–400 μm from the surface of the motor cortex (~150 nl each at a rate of 5–10 nl/min, controlled with BJ110 and BT200, BEX, using a pulled and beveled glass capillary B100-30-7.5HP and P-97, Sutter Instrument; EZP-60, Prime Tech). Following injection of the virus , the surface of the dura mater was cleaned with Gelfoam (Pfizer) soaked in artificial cerebrospinal fluid containing (in mM) 122 NaCl, 1.7 KCl, 1.1 $MgCl_2$, 23 $NaHCO_3$, 1.2 $CaCl_2$, 1.1 KH_2PO_4, and 3.4 glucose. The imaging window, a coverslip coated with Lipidure-CM5206 (NOF Corporation), was placed onto the dura mater and glued to the skull. Two miniature screws (TE-00003, Matsumoto Industry) were placed through the right frontal and parietal bones for EEG recording. Two stainless steel wires (AS633, Cooner Wire) were implanted into the neck muscle for electromyography (EMG) recording. A stainless-steel custom-made head-plate was glued to the skull to fix the head under the objective lens. After completion of the surgery, mice were returned to their home cages.

Fluorescence imaging

Fluorescence imaging was performed using a custom-designed upright two-photon laser-scanning microscope (based on Axio Examiner Z1/LSM780, with a water-immersion objective W Plan-Apochromat 20x/NA=1.0, Zeiss) (Nagayama et al. 2019). To observe spontaneous sleep/wake states in mice under the microscope, we used a spherical-treadmill system (Kanda et al. 2016). After recovery from surgery, the mice were acclimated to running and sleeping on the spherical-treadmill for 5 h during the light phase each day. The 5-day habituation allowed the mice to undergo spontaneous wake/NREM/REM sleep states on the spherical-treadmill during imaging (Fig 1). To maintain the brain temperature, the imaging window was superfused with saline at 37°C. Fluorescence was observed at layer 2/3 of the motor cortex (150–250 μm below the surface). GCaMP6s and tdTomato were two-photon excited at 910 and 1040 nm, respectively, using a tunable Ti:Sa laser (Maitai DeepSee, Spectra-Physics). The fluorescence of GCaMP6s and tdTomato was detected with a non-descanned GaAsP detector in the range of 500–550 nm and >555 nm, respectively (BiG, Zeiss). Excitation at 1040 nm was used to identify inhibitory neurons prior to time-lapse calcium imaging. Two-photon time-lapse images were intermittently acquired for approximately 2 h/day between 12:00 and 17:00 [Zeitgeber time (ZT) 3 and 7] at 8 frames/s with 128x256 pixels and 16-bit depth.

EEG/EMG recording and analysis

EEG and EMG signals were recorded during imaging experiments. EEG signals were amplified 40,000x and filtered with a pass-band of 0.5–500 Hz, and EMG signals were amplified 4000x and filtered with a pass-band of 1.5–1000 Hz using an analog amplifier (MEG-5200, NIHON KOHDEN). EEG/EMG signals were digitized at 2000 Hz using a 16-bit analog-to-digital converter (Digidata 1440A, Molecular Devices), and acquired with Clampex 10.3 software (Molecular Devices). The scan timing signals for the two-photon imaging were digitized with the same systems to temporally match the EEG/EMG data to the two-photon images. EEG and EMG signals were down-sampled at 250 Hz, divided into 4-s epochs, and sleep/wake states were scored in MATLAB (MathWorks). EEG power spectra were computed by a fast Fourier transform method to estimate slow-wave activity (SWA). Frequency resolution of power spectra was 1 Hz. SWA was defined as power density in the range of 2–4 Hz.

Sleep deprivation

Sleep deprivation (SD) experiments were performed at least 1 week after the spontaneous sleep/wake experiments. In some mice, the orders of these experiments were reversed. Imaged cells during SD and the following recovery sleep were the same as those imaged during spontaneous sleep/wake states of the

corresponding mouse. SD was induced by applying gentle air puffs to the face of the mice under the two-photon microscope (Fig 3A). The air puffs were randomly delivered every 3−7 s for 4 h (ZT3−6), which was controlled by a custom-made device (BEX). Two-photon imaging was performed for 3 h (ZT5−7), including 1 h after SD.

Histology

To confirm the selective expression of tdTomato in inhibitory (GABAergic) neurons in the motor cortex of Vgat-tdTomato mice, we performed fluorescence in situ hybridization (FISH) for GAD1 mRNA and immunohistochemistry (IHC) for tdTomato. Three Vgat-tdTomato mice (16–38 weeks old) were anesthetized with isoflurane and transcardially perfused with saline followed by 4% paraformaldehyde (PFA) in 0.1 M phosphate-buffered saline (PBS). The brains were post-fixed with the same fixative for at least 12 h at 4°C. After post-fixation, the brains were placed in 30% sucrose in PBS for at least 24 h and then stored with optimal cutting temperature compound (Tissue-Tek OTC compound, Sakura Finetek) at -80°C. The brains were sectioned coronally at a thickness of 40 μm with a cryostat (CM3050S, Leica). The sections were washed in 0.1 M phosphate buffer (PB) prior to the FISH/IHC procedures. All steps were performed at room temperature unless otherwise indicated. The brain sections containing the motor cortex were re-fixed with 4% PFA and permeabilized with 0.3% Triton X-100. The sections were treated with 1 μg/ml proteinase K at 37°C, 0.75% glycine, and 0.25% acetic anhydride. The treated sections were hybridized overnight at 60°C with a fluorescein isothiocyanate (FITC)-labeled probe for GAD1 mRNA. The hybridized sections were treated with RNase A at 37°C, and endogenous peroxidase activity was quenched with 0.3% H_2O_2 in tris-buffered saline (TBS). The sections were blocked with 1% blocking reagent (11096176001, Sigma-Aldrich/Roche) for 1 h, and sequentially incubated with a mouse anti-FITC antibody conjugated to horseradish peroxidase (1:80,000; 200-032-037, Jackson ImmunoResearch Laboratories) and a rabbit anti-red fluorescent protein (RFP) antibody (1:1000; PM005, Medical & Biological Laboratories) diluted in 1% blocking reagent/0.5% Triton X-100 in TBS at 4°C overnight. After washing with TNT (TBS, 0.15 M NaCl, and 0.05% Tween 20), horseradish peroxidase (HRP) signal was enhanced using the tyramide signal amplification biotin system (TSA Plus Biotin Kit, PerkinElmer). Following additional rinsing with TNT, the sections were incubated with a streptavidin-conjugated Alexa Fluor 488 (1:1000; S32354, Thermo Fisher Scientific/Molecular Probes) and an Alexa Fluor 594-conjugated anti-rabbit IgG antibody (1:1000; A-11012 or A-21207, Thermo Fisher Scientific/Molecular) diluted in 1% blocking reagent in TBS. After double FISH/IHC, the sections were rinsed three times with 0.1 M PB and mounted with antiphotobleaching medium (H-1200, Vector Labs). The fluorescence of Alexa Fluor 488 and 594 was imaged using a confocal laser scanning microscope (Axio Imager Z2 and

LSM700, Zeiss). Alexa Fluor 488- and 594-positive cells were defined as GAD1- and tdTomato-expressing cells, respectively.

Imaging data analysis

The fluorescence signal of each neuron in each frame (F_t) was estimated on the basis of the mean intensity across the pixels within each region of interest (ROI) after subtraction of the background signal using Fiji/ImageJ. The ROIs were set to exclude the neuropil signals. Because bleaching and motion artifacts were rarely observed, these corrections were not applied. The following analysis was performed with R (version 3.3.2) and python (3.6.0). To compare sleep/wake-state-dependent changes in fluorescence intensity between neurons, the F_t of each neuron was converted to a Z-score (F_z). The relative fluorescence signal $(\Delta F/F)_t$ was calculated for each ROI as follows:

$(\Delta F/F)_t = (F_t-F_o)/F_o$,

where F_o is the mean value of the lower 10% of F_t for all frames in one imaging file.

A sparse Gaussian Graphical Model (GGM) was used to model the local network structure from the two-photon images. GGM was specified by an inverse covariance matrix (i.e., the precision matrix Λ) of a multivariate Gaussian distribution. In GGM, the conditional independence between two nodes given other variables is equivalent to the corresponding entry in Λ ($\Lambda_{i,j}$) being zero. In other words, if $\Lambda_{i,j}$ is not zero, the conditional dependence is formed between two nodes and the entry indicates the strength of dependence. Because naïve estimation of the precision matrix leads to a dense matrix, which makes it difficult to see the essential connectivity, we imposed a sparsity-promoting regularization when estimating the precision matrix in GGM. The sparse precision matrix Λ was estimated using the R package glasso (graphical least absolute shrinkage and selection operator) (Friedman et al. 2007). In this report, the appearance and absolute value of the non-zero entry in the sparse precision matrix Λ were defined as the establishing connectivity and the strength of the established connectivity, respectively.

Because GGM assumes that the multivariate signals follow a multivariate Gaussian distribution, F_t was converted to F_s as follows:

$F_s = (\Delta F/F)_t-(\Delta F/F)_{t-1}$

The histogram of F_s revealed a Gaussian distribution (data not shown), supporting the use of GGM. The F_s data were segmented into 20-s epochs overlapping by 16 s, which were used to obtain the sparse precision matrix Λ at those time-points using glasso. Analysis was performed for each field of view. Thus, if M cells were observed in a field of view, Λ is a matrix of M rows and M columns. The glasso requires selecting a regularization parameter ρ to determine the degree of sparseness. To obtain an optimized Λ for local network analysis, ρ was determined for each field of view by comparison with visual inspection

analysis of ΔF/F. The number of neuron pairs showing changes in ΔF/F on at least one side (N_f) was compared with the number of established connectivity ($\Lambda_{i,j} \neq 0$) in GGM (N_g). This comparison was performed with data for wakefulness and NREM sleep, and ρ was determined so that $N_f / N_g \approx 1$ in both states (ρ = 0.0009–0.002). The probability of establishing connectivity in each pair (Pr) was calculated by dividing the number of epochs in which the corresponding non-zero entry in Λ appeared by the total number of epochs. The strength of the established connectivity in each pair (St) was calculated from the absolute value of the corresponding non-zero entry in Λ. St was normalized to [0,1] in all pairs for a single experiment. Two mice did not enter a sufficient amount of REM sleep (<80 s) for GGM analysis, and their data were excluded from network analysis of REM sleep. The number of samples for St differed from case to case because St was calculated from neuron pairs with $Pr \neq 0$.

Statistics

The data are expressed as mean ± standard deviation, unless otherwise indicated. The statistical tests were performed using R and JMP (SAS institute). Statistical tests are indicated in the result section. F_z values during each sleep/wake state were compared by Kruskal-Wallis test followed by Wilcoxon rank-sum test and Bonferroni correction (α=0.05/3). Classification based on activity profile of neurons was performed by comparing this test results with the average F_z value of each sleep/wake state. For example, W>N>R indicates that there are significant differences in F_z between three sleep/wake states (W, N, and R) by Kruskal-Wallis test and between all combinations of sleep/wake states (W−N, N−R, and R−W) by Wilcoxon rank-sum test and Bonferroni correction, and the average F_z during each state is W>N>R. Neurons that could not be classified in this test (e.g., no significant difference by Kruskal-Wallis Test) were named “unclassified”. The statistical significance tests used to analyze the connectivity were overly sensitive due to the large sample size of neuron pairs, and thus interpretation of the results focused on the distribution difference between groups. In quantile analysis, 1st, 2nd, 3rd, 4th indicate groups of $\{x>Q_3\}$, $\{Q_2<x\leq Q_3\}$, $\{Q_1<x\leq Q_2\}$, $\{x\leq Q_1\}$, respectively. Q_1, Q_2, and Q_3 indicate the first (lower 25%), second (50% or median), and third (upper 25%) quartiles, respectively. In some cases, the percentage of the 4th group was over 25% because the percentage of pairs of Pr=0 exceeded 25%.

Results

Neural Activity in the Motor Cortex is Lower during NREM sleep and Higher during REM sleep

To image cortical dynamics with cellular resolution in spontaneously sleeping and waking mice, we used two-photon microscopy with a spherical treadmill system (Fig 1A) (Kanda et al. 2016). Neural activity in layer 2/3 of the motor cortex was monitored using the genetically encoded calcium indicator GCaMP6s (Chen et al. 2013): an AAV vector encoding GCaMP6s under control of the neuron-specific human synapsin-1 promoter was injected into the superficial layer of the motor cortex. To overcome the technical limitations of spike width-based classification of cell types (Nowak et al. 2003), Vgat-tdTomato mice were generated (Materials and Methods). In Vgat-tdTomato mice, accurate and specific expression of tdTomato in inhibitory GABAergic neurons was histologically confirmed (Fig 1C, tdTomato+/Gad1+ cells, 98.9%; tdTomato+/Gad1- cells, 0.3%; tdTomato-/Gad1+ cells, 0.8%; n = 913 cells in the layer 2/3 of motor cortex from 3 mice). Therefore, GCaMP6s-only–expressing and GCaMP6s/tdTomato-expressing cells were defined as excitatory and inhibitory neurons, respectively (Fig 1B). Simultaneous recording of neural calcium signals, EEG, and EMG were performed during the mid-light phase (ZT3–8) (Fig 1D and 1E). In the two-photon images, the proportion of excitatory to inhibitory neurons was approximately 8:2, comparable with anatomic findings in the rodent cerebral cortex (DeFelipe et al. 2002). We first investigated whether sleep states affect spontaneous neural activity in the motor cortex. On the whole, the activity of excitatory neurons was lower during NREM sleep and higher during REM sleep compared with wakefulness (Fig 1F, all comparisons, $p < 0.001$, ANOVA followed by Tukey–Kramer test). The variability of mean neural activity per cell during wakefulness was equivalent to that during NREM sleep and smaller than that during REM sleep (Fig 1F, mean±SD of Z-scored fluorescence intensity (F_z), n = 783 cells; Wake, 0.22±0.18; NREM, -0.16±0.14; REM, 0.35±0.67). Inhibitory neurons and excitatory neurons exhibited a similar activity profile (Fig 1F, F_z, n = 193 cells; Wake, 0.25±0.19; NREM, -0.17±0.14; REM, 0.37±0.71; all comparisons, $p < 0.001$, ANOVA followed by Tukey–Kramer test). These results were broadly consistent with electrophysiological studies (Evarts 1964; Hobson and McCarley 1971; Vyazovskiy et al. 2009; Hengen et al. 2016; Watson et al. 2016). We next investigated the state in which individual neurons exhibited the highest activity (Fig 1G, see Materials and Methods). Approximately 30% of excitatory and inhibitory neurons exhibited the highest activity during wakefulness, and the subsequent level of activity was almost equally divided between NREM and REM sleep (Fig 1H). Approximately half of the excitatory and inhibitory neurons were REM-highest activity neurons, and >90% of REM-highest activity neurons exhibited the next highest level of activity for wakefulness (Fig 1H, R>W>N). Only 4−5% of excitatory and inhibitory neurons exhibited the highest activity during

NREM sleep, and, in >80% of the NREM-highest activity excitatory neurons, the next highest activity was observed in wakefulness (Fig 1H, N>W>R). In inhibitory neurons, N>W>R neurons accounted for 62.5% of NREM-highest activity neurons, which was less than the population of excitatory neurons. N>R>W, R>N>W, and N=R>W neurons comprised extremely small populations (N>R>W, 0.3% of Exc and 0.5% of Inh; R>N>W, 3.1% of Exc and 3.6% of Inh; N=R>W, 0.5% of Exc and 0.0% of Inh), suggesting that distinct neurons were relatively active in the motor cortex during NREM and REM sleep. In addition, the relative activity level during the state with maximum activity was significantly higher for REM-highest activity neurons than for Wake- or NREM-highest activity neurons (Fig 1I, $p < 0.001$, ANOVA followed by Tukey–Kramer test).

NREM Sleep Decreases and REM Sleep Increases Local Neural Connectivity

To clarify the dynamics of local network structures during sleep/wake states, we next investigated functional connectivity between neurons in the superficial layer of the motor cortex using sparse Gaussian graphical models (GGM). The structure of GGM was estimated by graphical least absolute shrinkage and selection operator (glasso) algorithm. GGM provides network graphs showing whether there is functional connectivity between neurons and, if there is, the strength of the connectivity. In this report, connectivity means that activities of two neurons are not independent of each other, taking into account not only linear correlations, but also several aspects of nonlinear relationships. To detect only essential connectivity, we imposed sparsity regularization to estimate the connectivity parameters in GGM. We quantified functional connectivity by "the probability of establishing connectivity in each pair (Pr)" and "the strength of the established connectivity in each pair (St)" (Materials and Methods). The network diagram in Fig 2A revealed that the number of established connectivity was decreased in NREM and increased in REM sleep compared with wakefulness. Mean Pr was highest in REM sleep, intermediate in wakefulness, and lowest in NREM sleep, and tended to be the same for any combination of cell types, but especially remarkable between inhibitory neurons (Fig 2B and 2C, mean Pr, Exc–Exc pair, 0.11±0.12 in W; 0.09±0.11 in N, 0.13±0.15 in R; Exc–Inh pair, 0.11±0.13 in W; 0.09±0.11 in N, 0.14±0.16 in R; Inh–Inh pair, 0.11±0.14 in W; 0.09±0.12 in N, 0.16±0.17 in R). Although St in NREM sleep had a relatively skewed distribution, the mean St did not drastically differ across the sleep/wake cycle (Fig 2B, mean St, Exc–Exc pair, 0.14±0.08 in W; 0.14±0.05 in N, 0.13±0.07 in R; Exc–Inh pair, 0.14±0.08 in W; 0.14±0.05 in N, 0.13±0.07 in R; Inh–Inh pair, 0.14±0.08 in W; 0.15±0.05 in N, 0.13±0.06 in R). The relationship between Pr and St for any pairs of cell types and any sleep/wake states was generally independent (Fig S1, the details of quantile-based rank order analysis are described below).

Neuron Pairs with Higher Probability of Establishing Connectivity Remain across the Sleep/Wake Cycle

To investigate the dynamics of the connectivity of each pair of neurons during sleep/wake states, neuron pairs were stratified into quartiles according to Pr or mean St (1st–4th indicate highest–lowest Pr and St pair in each state). The quantile-based rank order analysis indicates whether the relative rank of each pair by Pr and St within a local network vary across the states. If there is a clear proportional relationship between two states in a quantile-based 3D plot, the relative order of each pair by Pr or St within a local network does not change drastically between the two states, that is, neuron pairs with relatively high Pr or St in a state remain in another state. If there is no obvious trend between two states in a quantile-based 3D plots, the relative order of each pair by Pr or St within a local network tends to change drastically in the two states, that is, neuron pairs with relatively high Pr or St in a state do not remain in another state. In any pairs of cell types (Exc–Exc, Exc–Inh, and Inh–Inh), neuron pairs with a higher Pr had a relatively and consistently higher Pr across the sleep/wake cycles (Fig 2D, Wake-1st/NREM-1st Pr pairs, ≥15.1%; Wake-1st/REM-1st Pr pairs, ≥12.0%; NREM-1st/REM-1st Pr pairs, ≥15.4%), and similarly, neuron pairs with lower Pr had a relatively and consistently lower Pr across the sleep/wake cycles (Fig 2D, Wake-4th/NREM-4th Pr pairs, ≥14.6%; Wake-4th/REM-4th Pr pairs, ≥17.2%; NREM-4th/REM-4th Pr pairs, ≥20.6%), indicating that combination of neuron pairs with connectivity remain across the sleep/wake cycle. This tendency was much lower for St of any pairs across the sleep/wake cycle (Fig 2E, Wake-1st/NREM-1st St pairs, ≥12.6%; Wake-1st/REM-1st St pairs, ≥10.9%; NREM-1st/REM-1st St pairs, ≥11.9%; Wake-4th/NREM-4th St pairs, ≥12.6 %; Wake-4th/REM-4th St pairs, ≥10.8%; NREM-4th/REM-4th St pairs, ≥12.8 %), indicating that, although overall mean St does not change as a group (Fig 2B), relative strength of connectivity in each neuron pair within a network change drastically across the sleep/wake cycle.

Sleep Deprivation Strengthens Local Cortical Connectivity

Sleep is homeostatically regulated: forced wakefulness is followed by recovery sleep. To investigate whether SD affects local cortical connectivity, we designed a method to produce SD under the microscope (Fig 3A). SD was performed from ZT3 to ZT6, and imaging was performed from ZT5 to ZT7 (Fig 3B). Random delivery of an air puff to the mouse face efficiently disrupted NREM sleep (Fig 3C and 3D, % of NREM sleep at ZT5−6, 61.4±4.5% in the absence of SD, 11.3±6.3% in the presence of SD, n = 5 mice, $p<0.003$, paired t-test). The SD experiments were performed with some of the same mice used in spontaneous sleep/wake experiments (Figs 1 and 2), and the same fields of view were imaged. Therefore, in the following analysis of SD experiment data, the same cells were compared in the presence or absence of SD. Neural activity of excitatory neurons was slightly, but significantly, lower in wakefulness during

SD than in spontaneous wakefulness without SD (no SD condition) (Fig 3F, mean $(\Delta F/F)_t$ for wakefulness at ZT5–6, 0.68±0.46 without SD, 0.55±0.36 with SD, n = 539 cells, $p < 0.0001$, Wilcoxon signed rank test). SD did not affect neural activity of inhibitory neurons (Fig 3F, mean $(\Delta F/F)_t$ for wakefulness at ZT5–6, 0.56±0.38 without SD, 0.49±0.22 with SD, n = 120 cells, p = 0.20, Wilcoxon signed rank test). Connectivity was largely altered during SD (Fig 3G). An increase in Pr during SD was observed only in inhibitory neurons, not in the excitatory neurons (Fig 3H, median of Pr, Exc–Exc pair, 0.06 in W without SD, 0.06 in W during SD, n = 31,422 pairs; Exc–Inh pair, 0.06 in W no SD, 0.09 in W during SD, n = 12,740 pairs; Inh-Inh pair, 0.04 in W no SD, 0.14 in W during SD, n = 1412 pairs). St during SD was increased in both excitatory and inhibitory neurons, but prominently in inhibitory neurons (Fig 3I, median of St, Exc–Exc pair, 0.12 in W no SD, 0.14 in W during SD, n = 18,458 pairs; Exc–Inh pair, 0.13 in W no SD, 0.16 in W during SD, n = 8096 pairs; Inh-Inh pair, 0.14 in W no SD, 0.20 in W during SD, n = 853 pairs). These results suggest that extended wakefulness strengthens associated activity between cortical neurons.

Recovery Sleep Weakens Local Cortical Connectivity

We next analyzed neural connectivity during recovery sleep (NREM sleep at ZT7 after SD). EEG slow-wave activity (SWA, EEG power density in the range of 2-4 Hz) during NREM sleep was increased after SD (Fig 4C, 38.0% in the absence of SD, 41.6% in the presence of SD, n = 5 mice, p = 0.013, paired t-test), indicating an increase in sleep pressure (Borbély 1982). Neural activity of excitatory and inhibitory neurons during NREM sleep at ZT7 was not affected by the presence or absence of SD (no SD condition) (Exc, 0.37±0.15 without SD, 0.35±0.16 with SD, n = 539 cells, p = 0.06, Wilcoxon signed rank test; Inh, 0.33±0.12 without SD, 0.32±0.14 with SD, n = 120 cells, p = 0.51, Wilcoxon signed rank test). Neural activity during NREM sleep was not affected by the presence or absence of SD, whereas neural connectivity during NREM sleep following SD largely differed from that without SD (Fig 4D). Pr during NREM sleep following SD exhibited complicated changes compared with the no SD condition: the median Pr was decreased in excitatory neurons, but not in inhibitory neurons (Fig 4E, Pr median, Exc–Exc pair, 0.06 in N no SD, 0.02 in N after SD; Exc–Inh pair, 0.05 in N no SD, 0.02 in N after SD; Inh-Inh pair, 0.03 in N no SD, 0.03 in N after SD), in addition, the upper quantile (Q_3) of Pr was decreased in excitatory neurons and increased in inhibitory neurons (Fig 4F, Q_3 of Pr, Exc–Exc pair, 0.15 in N no SD, 0.09 in N after SD; Exc–Inh pair, 0.16 in N no SD, 0.12 in N after SD; Inh-Inh pair, 0.18 in N no SD, 0.23 in N after SD). Unlike Pr, St during NREM sleep following SD was decreased regardless of cell type (Fig 4F, median (Q_2) and lower quantile (Q_1) of Pr, Exc–Exc pair, 0.18 and 0.15 in N no SD, 0.17 and 0.11 in N after SD; Exc–Inh pair, 0.18 and 0.15 in N no SD, 0.18 and 0.12 in N after SD; Inh-Inh pair, 0.18 and 0.16 in N no

SD, 0.17 and 0.12 in N after SD), suggesting that the strengthened connectivity between cortical neurons during extended wakefulness is weakened during recovery sleep by homeostatic mechanisms.

Homeostatic Regulation of Individual Connectivity

To investigate how the connectivity of each neuron pair changes in sleep homeostasis, neuron pairs were stratified into quartiles on the basis of the mean Pr or St (same as Fig 2D and 2E). Excitatory, but not inhibitory, neuron pairs with lower Pr during wakefulness maintained a lower Pr during SD (Fig 5A, % of W-during-SD-4th/W-no-SD-4th Pr pairs, 21.8% in Exc-Exc; 15.5% in Exc-Inh; 12.8% in Inh-Inh), indicating that Pr between excitatory neurons is not affected by SD not only in terms of the group (Fig 3H), but also in term of individual pairs. There was not a clear trend of Pr between NREM sleep in the presence or absence of SD (Fig 5A), indicating that combination of neuron pairs with connectivity during NREM sleep do not remain after SD. Inhibitory, but not excitatory, neuron pairs with relatively high Pr within a local network during SD remained during the following recovery sleep (Fig 5A, % of W-during-SD-1st/NREM-after-SD-1st Pr pairs, 10.8% in Exc-Exc; 16.3% in Exc-Inh; 19.1% in Inh-Inh). The quantile-based rank order analysis of St did not exhibit an obvious tendency between wakefulness during SD and without SD, and between NREM sleep after SD and without SD (Fig 5B), which was similar to those of St across spontaneous sleep/wake states (Fig 2E). Neuron pairs with a higher St during SD exhibited higher St during the following recovery sleep (Fig 5B, % of W-during-SD-1st/NREM-after-SD-1st Pr pairs, 15.8% in Exc-Exc; 16.8% in Exc-Inh; 17.6% in Inh-Inh), indicating that relative strength of connectivity of each neuron pairs in any neuron type within a local network does not change largely during prolonged wakefulness and the following recovery sleep.

Characteristic Spatial Patterns Emerges in Inhibitory Connectivity

We next investigated the spatial properties of connectivity. Neuron pairs were divided into four groups according to the distance between neurons (the percentage of pairs at each distance, 24.1–33.7% at <100 μm; 34.6–45.8% at 100−200 μm; 16.5−26.0% at 200–300 μm; and 3.5–15.1% at >300 μm). Fig 6A and 6B show the proportion of neuron pairs stratified into quartiles on the basis of Pr and St at that distance. Characteristic spatial patterns of local connectivity emerged in inhibitory networks, but not excitatory networks, for NREM and REM sleep. Inhibitory neuron pairs with a distance of >300 μm exhibited relatively higher Pr during sleep, especially REM sleep (Fig 6A, at a distance of >300 μm, 1st-Pr Exc–Exc pairs, 29.4% in W, 32.5% in N, 27.9% in R; 1st-Pr Exc–Inh pairs, 30.4% in W, 33.6% in N, 27.4% in R; 1st-Pr Inh–Inh pairs, 26.5% in W, 35.5% in N, 40.4% in R). On the other hand, we did not detect a clear relationship between St and the distance between neurons during spontaneous sleep/wake states (Fig

6B). These findings suggest that inhibitory neurons tend to show connectivity with non-adjacent neurons rather than with neighboring neurons during REM sleep. SD also induced characteristic spatial properties of local cortical connectivity (Fig 6). Neuron pairs with higher Pr were rarely observed in inhibitory neurons with a distance of >300 μm during SD (Fig 6A, at a distance of >300 μm, 1st-Pr pairs in W during SD, 21.6% in Exc-Exc, 16.3% in Exc-Inh, 12.9% in Inh-Inh). Neuron pairs with higher St were infrequent in both excitatory and inhibitory neurons with a distance of >300 μm, (Fig 6B, at a distance of >300 μm, 1st-St pairs in W during SD, 11.8% in Exc-Exc, 10.1% in Exc-Inh,12.5% in Inh-Inh). These observations suggest that extended wakefulness decreases and weakens non-adjacent neural connectivity. In NREM sleep following SD, neuron pairs with higher Pr were hardly ever observed in distant neurons (Fig 6A, at a distance of >300 μm, 1st-Pr pairs in N following SD, 9.9% in Exc-Exc, 9.6% in Exc-Inh, 6.2% in Inh-Inh). A lower proportion of neuron pairs with higher St in distant neurons was observed in inhibitory, but not excitatory, neurons (Fig 6B, at a distance of >300 μm, 1st-St pairs in N following SD, 21.0% in Exc-Exc, 25.0% in Exc-Inh, 16.2% in Inh-Inh), suggesting that neural connectivity was rarely established between non-adjacent neurons during recovery sleep.

Discussion

In this study using calcium imaging, we found that individual neural activity was decreased during NREM sleep, increased during REM sleep, slightly suppressed during extended wakefulness, and not significantly affected by subsequent recovery sleep. To investigate neural connectivity from calcium imaging data, we applied GGM and estimated neural connectivity using the glasso algorithm, and revealed that local cortical connectivity was sparse in NREM sleep and dense in REM sleep. SD induced strong connectivity, whereas subsequent homeostatic recovery sleep induced weak and sparse connectivity. Figure 7 summarizes changes in connectivity across sleep/wake cycles and during the homeostatic process. Quantile-based rank order analysis showed that the relative rank of the St of each neuron pair within a local network (field-of-view of 425.10 μm x 212.55 μm) varied across spontaneous sleep/wake states, which was also observed during and after SD. Changes in the relative rank of Pr of each neuron pair within a local network were not observed across spontaneous sleep/wake states, but only during and after SD. Spatial analysis revealed that connectivity between non-adjacent inhibitory neurons was dense during REM sleep and sparse during and after SD. Neural connectivity between non-adjacent excitatory/inhibitory neurons was weakened during SD and sparse during the following recovery sleep.

Diverse patterns of individual cortical neuron activity during sleep/wake states

A large majority (>90%) of neurons exhibited the highest activity during wakefulness or REM sleep, consistent with findings from extracellular unit recording studies (Evarts 1964; Hobson and McCarley 1971; Vyazovskiy et al. 2009; Hengen et al. 2016; Watson et al. 2016) and a two-photon calcium imaging study on pyramidal cells in the layer 5 of barrel cortex (Seibt et al. 2017). A small population (≈5%) showed the highest activity during NREM sleep. Multi-unit recordings of a large number of neurons indicate that a small number of cortical low-frequency firing neurons slightly increases their firing rate in NREM sleep (Watson et al. 2016). Indeed, the relative activity in the state showing the maximum activity tended to be lower in NREM-highest activity neurons than in the Wake- or REM-highest activity neurons, suggesting that NREM-highest activity neurons could contain low-frequency firing neurons. Wide-field calcium imaging reveals atypical activity: activity of cortical pyramidal neurons is globally reduced in NREM sleep and further suppressed in REM sleep (Niethard et al. 2016). This type of activity (W>N>R active) was not the major pattern, but appeared in 15.6% of excitatory neurons in our study. Although there were no large differences in activity of excitatory and inhibitory neurons across the sleep/wake cycles, each has various subtypes whose activity level differed from state to state. Recent calcium imaging studies revealed that parvalbumin- and somatostatin-expressing inhibitory neurons exhibit distinct changes in activity during sleep/wake states (Niethard et al. 2016, 2018). Changes in activity of cortical neurons

during sleep/wake states are thought to be caused by volume transmission of neuromodulators and wired transmission from the thalamus (Steriade et al. 1993; Kanda et al. 2017). Since the diversity of the changes shown in this report cannot be explained by known mechanisms, intrinsic mechanisms, such as membrane properties, might contribute to changes in individual neural activity across sleep/wake states. Although SD increases SWA in EEG (Borbély 1982), individual neural activity was largely not changed, suggesting that the increase in SWA in EEG is not simply correlated with changes in individual neural activity during extended wakefulness and following recovery sleep. These findings are consistent with those from an optogenetic study in which optogenetic stimulation of cortical neurons does not increase SWA in EEG (Rodriguez et al. 2016). Our observations of neural activity during and after SD are consistent with a previous electrophysiological study indicating negligible changes in firing of cortical neurons after 1-h SD with gentle handling (Hengen et al. 2016) and inconsistent with another electrophysiological study in the cortex demonstrating an increase in firing rates during 4-h SD with novel objects or acoustic stimuli (Vyazovskiy et al. 2009) and ; the discrepancy might be due to the difference in the duration and method of SD.

Functional relevance of local connectivity dynamics during sleep/wake states

In the motor cortex, neural signals are basically derived from thalamocortical and corticocortical inputs to local recurrent circuits in the superficial layer (layer 2/3) and transferred to the deep layer for outputs (Weiler et al. 2008); thus, modulation of the local connectivity within the superficial layer is thought to be required for learning new motor tasks. In fact, both morphological and functional plasticity occur in the motor cortex following motor learning (Rioult-Pedotti et al. 1998; Peters et al. 2014; Yang et al. 2014; Biane et al. 2016; Li et al. 2017). In addition, post-motor task NREM sleep promotes the formation of dendritic spines in the motor cortex (Gulati et al. 2014, 2017; Yang et al. 2014). The ability to induce further long-term synaptic potentiation (LTP), however, is nearly saturated in the motor cortex after learning (Rioult-Pedotti et al. 1998). For desaturation of synaptic potentiation, NREM sleep is generally hypothesized to weaken synaptic strength (Tononi and Cirelli 2014). Indeed, synaptic structures are downscaled in NREM sleep without specific tasks (Maret et al. 2011; de Vivo et al. 2017; Diering et al. 2017). The physiological events that underlie downscaling of synaptic efficacy during NREM sleep, however, are unknown.

Our calcium imaging and statistical learning approach revealed that functional connectivity within the motor cortex superficial layer was sparse during NREM sleep. Establishing functional connectivity reflects an increase in local synaptic interactions or common afferent inputs that are thought to be linked with synaptic plasticity and cell assembly (Hebb 1949). Assuming that establishing connectivity results in

synaptic plasticity, sparse connectivity during NREM sleep could contribute to a reduction in potentiated synaptic efficacy because, in general, low-frequency transmission induces depotentiation of existing LTP (Martin et al. 2000; Neves et al. 2008). In addition, SD prevents improvement of motor skills after training (Stickgold 2005). Local cortical networks exhibited stronger connectivity between excitatory neurons during SD, which might contribute to preventing depotentiation of potentiated synapses. Because the probability of establishing connectivity in excitatory neurons was not changed by SD, SD might not allow for the formation of new spines. Indeed, SD decreases spine disappearance but does not increase the formation of spines in the adolescent cortex (Maret et al. 2011). SD-induced strong connectivity might disrupt motor learning due to excessive synaptic plasticity. Thus, taken together, it is possible that NREM sleep restores the ability to acquire new memory through resetting potentiated synapses due to the sparse neural connectivity. In addition, sparse connectivity in NREM sleep contribute to induction of synaptic plasticity at specific synapses. If neurons that activate in response to specific tasks reactivate during subsequent NREM sleep, the reactivating neurons may establish strong functional connectivity, which is likely to cause plastic changes at synapses between the reactivating neurons because the reactivating synaptic interactions are relatively conspicuous in the sparse connectivity environment caused by NREM sleep. In fact, spine formation after motor learning is likely to occur in neurons that reactivate during NREM sleep (Yang et al. 2014). After SD, excitatory neurons exhibited sparse and weak connectivity, which may play a homeostatic role in resetting the ability to induce motor learning. SD also caused dense connectivity in inhibitory neurons, but not excitatory neurons. SD is a risk factor for epileptic activity (Malow 2004). Dense, strong, and adjacent inhibitory connectivity could suppress excessive excitatory activity caused by the strong connectivity established during SD.

REM sleep eliminates newly formed excessive spines and increases the size of persistent new spines in the motor cortex after motor learning (Li et al. 2017). Such upregulation of synaptic efficacy in a fraction of synapses is considered necessary to maintain new memory for motor skills. In fact, artificial depotentiation of potentiated spines after motor learning disrupts performance of learned motor skills (Hayashi-Takagi et al. 2015). Therefore, the dense connectivity established during REM sleep might contribute to maintain acquired motor skills for a certain period of time by preventing depotentiation. Inhibitory neurons in REM sleep exhibited a marked increase in connectivity with other neurons and the paired partners were a bit further away, which could affect inhibitory network-specific plasticity in the motor cortex that is required for learning (Donato et al. 2013; Chen et al. 2015) and control functional stability of cortical excitatory plasticity over a long period of time (Mongillo et al. 2018).

An ultimate goal of sleep research is to understand the phenomenon of sleep from cellular activity, beyond EEG and behaviors. In this study, we found sleep/wake state-dependent dynamics of functional

connectivity at the second level. Such a slow modulation is a prominent feature of sleep (Crunelli and Hughes 2010). However our analysis may miss short-term changes in firing patterns or synchronization at the millisecond level (Steriade et al. 1996, 2001), because the temporal resolution of calcium imaging is not yet comparable with that of electrophysiological recordings. In addition, glasso algorism can limit minor connectivity, but cannot detect the direction of connectivity. Further understanding requires the development of new experimental and statistical methods.

Acknowledgments

We thank M. Kakizaki and Y. Ishikawa for preparing the materials. We also thank M. Sato, H. Sekiya, N. Kitajima, K. Satoh, and K. Vogt for technical advice. This work was supported by Grants-in-Aid for Scientific Research (KAKENHI), Japan Society for the Promotion of Science (JSPS) (Grant Number 16K18358 to T.K.; 26220207 to T.K. and M.Y.; 26507002 and 25293247 to N.T.; 19K12111 to H.H; 17H06095 to M.Y.); Funding Program for World-Leading Innovative R&D on Science and Technology (FIRST program), JSPS (to M.Y.); World Premier International Research Center Initiative (WPI), the Ministry of Education, Culture, Sports, Science and Technology (MEXT) (to M.Y.); Core Research for Evolutional Science and Technology (CREST), Japan Science and Technology Agency (JST) (Grant Number JPMJCR1761 to H.H.; JPMJCR1655 to M.Y.); Yamada Research Grant (to T.K.), Takeda Science Foundation (to M.Y.), and Uehara Memorial Foundation (to M.Y.).

DECLARATION OF INTERESTS

The authors declare no competing interests.

REFERENCES

Biane JS, Takashima Y, Scanziani M, Conner JM, Tuszynski MH. 2016. Thalamocortical Projections onto Behaviorally Relevant Neurons Exhibit Plasticity during Adult Motor Learning. Neuron. 89:1173–1179.

Borbély AA. 1982. A two process model of sleep regulation. Hum Neurobiol. 1:195–204.

Chen SX, Kim AN, Peters AJ, Komiyama T. 2015. Subtype-specific plasticity of inhibitory circuits in motor cortex during motor learning. Nat Neurosci. 18:1109–1115.

Chen T-W, Wardill TJ, Sun Y, Pulver SR, Renninger SL, Baohan A, Schreiter ER, Kerr R a., Orger MB, Jayaraman V, Looger LL, Svoboda K, Kim DS. 2013. Ultrasensitive fluorescent proteins for imaging neuronal activity. Nature. 499:295–300.

Chow HM, Horovitz SG, Carr WS, Picchioni D, Coddington N, Fukunaga M, Xu Y, Balkin TJ, Duyn JH, Braun AR. 2013. Rhythmic alternating patterns of brain activity distinguish rapid eye movement sleep from other states of consciousness. Proc Natl Acad Sci. 110:10300–10305.

Crunelli V, Hughes SW. 2010. The slow (<1 Hz) rhythm of non-REM sleep: a dialogue between three cardinal oscillators. Nat Neurosci. 13:9–17.

de Vivo L, Bellesi M, Marshall W, Bushong EA, Ellisman MH, Tononi G, Cirelli C. 2017. Ultrastructural evidence for synaptic scaling across the wake/sleep cycle. Science (80-). 355:507–510.

DeFelipe J, Alonso-Nanclares L, Arellano JI. 2002. Microstructure of the neocortex: Comparative aspects. J Neurocytol. 31:299–316.

Diering GH, Nirujogi RS, Roth RH, Worley PF, Pandey A, Huganir RL. 2017. Homer1a drives homeostatic scaling-down of excitatory synapses during sleep. Science (80-). 355:511–515.

Dobra A, Hans C, Jones B, Nevins JR, Yao G, West M. 2004. Sparse graphical models for exploring gene expression data. J Multivar Anal. 90:196–212.

Donato F, Rompani SB, Caroni P. 2013. Parvalbumin-expressing basket-cell network plasticity induced by experience regulates adult learning. Nature. 504:272–276.

Evarts E V. 1964. Temporal patterns of discharge of pyramidal tract neurons during sleep and waking in the monkey. J Neurophysiol. 27:152–171.

Friedman J, Hastie T, Tibshirani R. 2007. Sparse inverse covariance estimation with the lasso. Biostatistics. 9:432–441.

Gulati T, Guo L, Ramanathan DS, Bodepudi A, Ganguly K. 2017. Neural reactivations during sleep determine network credit assignment. Nat Neurosci. 20:1277–1284.

Gulati T, Ramanathan DS, Wong CC, Ganguly K. 2014. Reactivation of emergent task-related ensembles during slow-wave sleep after neuroprosthetic learning. Nat Neurosci. 17:1107–1113.

Hayashi-Takagi A, Yagishita S, Nakamura M, Shirai F, Wu YI, Loshbaugh AL, Kuhlman B, Hahn KM, Kasai H. 2015. Labelling and optical erasure of synaptic memory traces in the motor cortex. Nature. 525:333–338.

Hebb DO. 1949. The organization of behavior; a neuropsychological theory. Oxford: Wiley.

Hengen KB, Torrado Pacheco A, McGregor JN, Van Hooser SD, Turrigiano GG. 2016. Neuronal Firing Rate Homeostasis Is Inhibited by Sleep and Promoted by Wake. Cell. 165:180–191.

Hobson JA, McCarley RW. 1971. Cortical unit activity in sleep and waking. Electroencephalogr Clin Neurophysiol. 30:97–112.

Holtmaat A, Bonhoeffer T, Chow DK, Chuckowree J, De Paola V, Hofer SB, Hübener M, Keck T, Knott G, Lee W-CA, Mostany R, Mrsic-Flogel TD, Nedivi E, Portera-Cailliau C, Svoboda K, Trachtenberg JT, Wilbrecht L. 2009. Long-term, high-resolution imaging in the mouse neocortex through a chronic cranial window. Nat Protoc. 4:1128–1144.

Horovitz SG, Braun AR, Carr WS, Picchioni D, Balkin TJ, Fukunaga M, Duyn JH. 2009. Decoupling of the brain's default mode network during deep sleep. Proc Natl Acad Sci. 106:11376–11381.

Huber R, Ghilardi MF, Massimini M, Ferrarelli F, Riedner BA, Peterson MJ, Tononi G. 2006. Arm immobilization causes cortical plastic changes and locally decreases sleep slow wave activity. Nat Neurosci. 9:1169–1176.

Huber R, Ghilardi MF, Massimini M, Tononi G. 2004. Local sleep and learning. Nature. 430:78–81.

Kanda T, Ohyama K, Muramoto H, Kitajima N, Sekiya H. 2017. Promising techniques to illuminate neuromodulatory control of the cerebral cortex in sleeping and waking states. Neurosci Res. 118:92–103.

Kanda T, Tsujino N, Kuramoto E, Koyama Y, Susaki EA, Chikahisa S, Funato H. 2016. Sleep as a biological problem: an overview of frontiers in sleep research. J Physiol Sci. 66:1–13.

Kawai R, Markman T, Poddar R, Ko R, Fantana AL, Dhawale AK, Kampff AR, Ölveczky BP. 2015. Motor Cortex Is Required for Learning but Not for Executing a Motor Skill. Neuron. 86:800–812.

Kishino H, Waddell PJ. 2000. Correspondence analysis of genes and tissue types and finding genetic links from microarray data. Genome Inform Ser Workshop Genome Inform. 11:83–95.

Koike T, Kan S, Misaki M, Miyauchi S. 2011. Connectivity pattern changes in default-mode network with deep non-REM and REM sleep. Neurosci Res. 69:322–330.

Li W, Ma L, Yang G, Gan W-B. 2017. REM sleep selectively prunes and maintains new synapses in development and learning. Nat Neurosci. 20:427–437.

Madisen L, Zwingman T a, Sunkin SM, Oh SW, Zariwala HA, Gu H, Ng LL, Palmiter RD, Hawrylycz MJ, Jones AR, Lein ES, Zeng H. 2010. A robust and high-throughput Cre reporting and characterization system for the whole mouse brain. Nat Neurosci. 13:133–140.

Malow BA. 2004. Sleep deprivation and epilepsy. Epilepsy Curr. 4:193–195.

Maret S, Faraguna U, Nelson AB, Cirelli C, Tononi G. 2011. Sleep and waking modulate spine turnover in the adolescent mouse cortex. Nat Neurosci. 14:1418–1420.

Martin SJ, Grimwood PD, Morris RGM. 2000. Synaptic Plasticity and Memory: An Evaluation of the Hypothesis. Annu Rev Neurosci. 23:649–711.

Mongillo G, Rumpel S, Loewenstein Y. 2018. Inhibitory connectivity defines the realm of excitatory plasticity. Nat Neurosci. 21:1463–1470.

Mostany R, Portera-Cailliau C. 2008. A craniotomy surgery procedure for chronic brain imaging. J Vis Exp. 680.

Nagayama M, Aritake T, Hino H, Kanda T, Miyazaki T, Yanagisawa M, Akaho S, Murata N. 2019. Sleep State Analysis Using Calcium Imaging Data by Non-negative Matrix Factorization. In: Tetko Igor V.,, Kůrková Věra,, Karpov Pavel,, Theis Fabian, editors. Artificial Neural Networks and Machine Learning – ICANN 2019: Theoretical Neural Computation. ICANN 2019. Lecture Notes in Computer Science. Lecture Notes in Computer Science. Cham: Springer, Cham. p. 102–113.

Neves G, Cooke SF, Bliss TVP. 2008. Synaptic plasticity, memory and the hippocampus - a neural network aproach to causality. Nat Rev Neurosci. 9:65–75.

Niethard N, Hasegawa M, Itokazu T, Oyanedel C, Born J, Sato T. 2016. Sleep-Stage-Specific Regulation of Cortical Excitation and Inhibition. Curr Biol. 26:2739–2749.

Niethard N, Ngo H-V V., Ehrlich I, Born J. 2018. Cortical circuit activity underlying sleep slow oscillations and spindles. Proc Natl Acad Sci. 115:E9220–E9229.

Nowak LG, Azouz R, Sanchez-Vives M V, Gray CM, McCormick D a. 2003. Electrophysiological classes of cat primary visual cortical neurons in vivo as revealed by quantitative analyses. J Neurophysiol. 89:1541–1566.

Peters AJ, Chen SX, Komiyama T. 2014. Emergence of reproducible spatiotemporal activity during motor learning. Nature. 510:263–267.

Peters AJ, Liu H, Komiyama T. 2017. Learning in the Rodent Motor Cortex. Annu Rev Neurosci. 40:77–97.

Picchioni D, Duyn JH, Horovitz SG. 2013. Sleep and the functional connectome. Neuroimage. 80:387–396.

Ramanathan DS, Gulati T, Ganguly K. 2015. Sleep-Dependent Reactivation of Ensembles in Motor Cortex Promotes Skill Consolidation. PLOS Biol. 13:e1002263.

Rioult-Pedotti MS, Friedman D, Hess G, Donoghue JP. 1998. Strengthening of horizontal cortical connections following skill learning. Nat Neurosci. 1:230–234.

Rodriguez A V., Funk CM, Vyazovskiy V V., Nir Y, Tononi G, Cirelli C. 2016. Why Does Sleep Slow-Wave Activity Increase After Extended Wake? Assessing the Effects of Increased Cortical Firing During Wake and Sleep. J Neurosci. 36:12436–12447.

Rosa MJ, Portugal L, Hahn T, Fallgatter AJ, Garrido MI, Shawe-Taylor J, Mourao-Miranda J. 2015. Sparse network-based models for patient classification using fMRI. Neuroimage. 105:493–506.

Sämann PG, Wehrle R, Hoehn D, Spoormaker VI, Peters H, Tully C, Holsboer F, Czisch M. 2011. Development of the brain's default mode network from wakefulness to slow wave sleep. Cereb Cortex. 21:2082–2093.

Sanes JN, Donoghue JP. 2000. Plasticity and primary motor cortex. Annu Rev Neurosci. 23:393–415.

Seibt J, Richard CJ, Sigl-Glöckner J, Takahashi N, Kaplan DI, Doron G, de Limoges D, Bocklisch C, Larkum ME. 2017. Cortical dendritic activity correlates with spindle-rich oscillations during sleep in rodents. Nat Commun. 8:684.

Siclari F, Tononi G. 2017. Local aspects of sleep and wakefulness. Curr Opin Neurobiol. 44:222–227.

Spoormaker VI, Gleiser PM, Czisch M. 2012. Frontoparietal connectivity and hierarchical structure of the brain's functional network during sleep. Front Neurol. MAY:1–10.

Steriade M, Amzica F, Contreras D. 1996. Synchronization of fast (30-40 Hz) spontaneous cortical rhythms during brain activation. J Neurosci. 16:392–417.

Steriade M, McCormick D a, Sejnowski TJ. 1993. Thalamocortical oscillations in the sleeping and aroused brain. Science. 262:679–685.

Steriade M, Timofeev I, Grenier F. 2001. Natural waking and sleep states: a view from inside neocortical neurons. J Neurophysiol. 85:1969–1985.

Stickgold R. 2005. Sleep-dependent memory consolidation. Nature. 437:1272–1278.

Toh H, Horimoto K. 2002. Inference of a genetic network by a combined approach of cluster analysis and graphical Gaussian modeling. Bioinformatics. 18:287–297.

Tononi G, Cirelli C. 2014. Sleep and the Price of Plasticity: From Synaptic and Cellular Homeostasis to Memory Consolidation and Integration. Neuron. 81:12–34.

Vong L, Ye C, Yang Z, Choi B, Chua S, Lowell BB. 2011. Leptin action on GABAergic neurons prevents obesity and reduces inhibitory tone to POMC neurons. Neuron. 71:142–154.

Vyazovskiy V V, Harris KD. 2013. Sleep and the single neuron: the role of global slow oscillations in individual cell rest. Nat Rev Neurosci. 14:1–9.

Vyazovskiy V V, Olcese U, Lazimy YM, Faraguna U, Esser SK, Williams JC, Cirelli C, Tononi G. 2009. Cortical Firing and Sleep Homeostasis. Neuron. 63:865–878.

Watson BO, Levenstein D, Greene JP, Gelinas JN, Buzsáki G. 2016. Network Homeostasis and State Dynamics of Neocortical Sleep. Neuron. 90:839–852.

Weiler N, Wood L, Yu J, Solla SA, Shepherd GMG. 2008. Top-down laminar organization of the excitatory network in motor cortex. Nat Neurosci. 11:360–366.

Wu CW, Liu P-Y, Tsai P-J, Wu Y-C, Hung C-S, Tsai Y-C, Cho K-H, Biswal BB, Chen C-J, Lin C-P. 2012. Variations in Connectivity in the Sensorimotor and Default-Mode Networks During the First Nocturnal Sleep Cycle. Brain Connect. 2:177–190.

Yang G, Lai CSW, Cichon J, Ma L, Li W, Gan W-B. 2014. Sleep promotes branch-specific formation of dendritic spines after learning. Science (80-). 344:1173–1178.

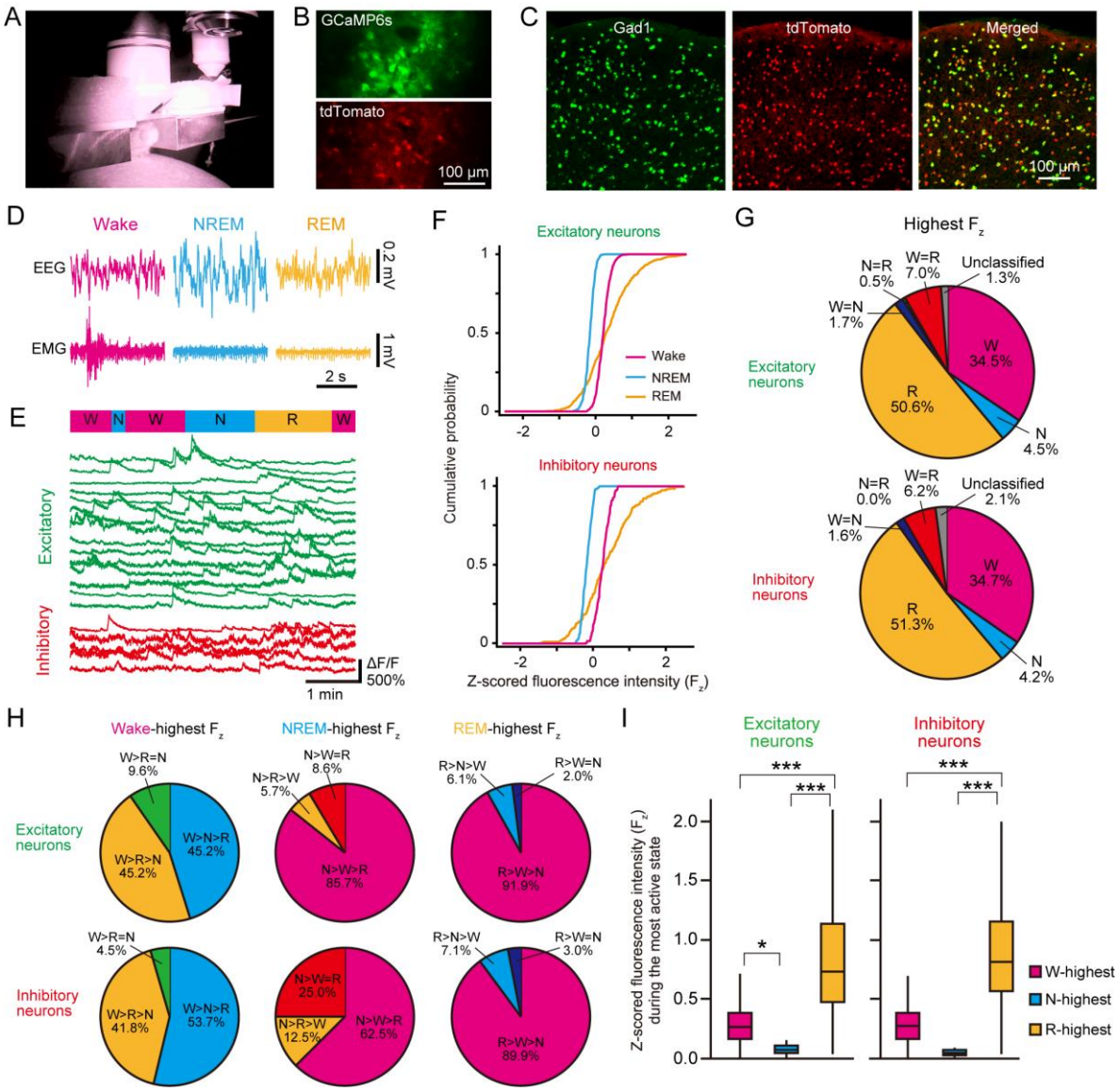

Figure 1. **Calcium imaging of excitatory and inhibitory neurons in the motor cortex during sleep and wakefulness.** (A) An infrared camera image depicting a mouse on a spherical treadmill during two-photon imaging. (B) Two-photon images of GCaMP6s (upper, green) and tdTomato (lower, red) in layer 2/3 of the motor cortex in a Vgat-tdTomato mouse injected with rAAV2/9-hSyn-GCaMP6s-WPRE. (C) Representative confocal images of fluorescence in situ hybridization for Gad1 mRNA (left, green) and immunohistochemistry for tdTomato (middle, red) in the motor cortex of a Vgat-tdTomato mouse. Merged image of the left and middle panels shows colocalization (Right). (D) EEG and EMG during two-photon imaging reflecting sleep/wake states: desynchronized EEG and high-amplitude EMG during wakefulness (magenta), high-amplitude slow-wave EEG and lower-amplitude EMG during NREM sleep (cyan), and theta-frequency EEG and much lower-amplitude EMG during REM sleep (orange). (E) Representative relative fluorescence intensity (ΔF/F)t of GCaMP6s in sleep/wake cycles. Green and red traces indicate ΔF/F of excitatory and inhibitory neurons, respectively. Top color bar denotes the sleep/wake state of the

mouse: wakefulness (W, magenta), NREM (N, cyan), and REM sleep (R, orange). (F) Cumulative distribution of mean z-scored fluorescence intensity (F_z) per cell of excitatory (upper, n = 783 cells) and inhibitory neurons (lower, n = 193 cells) during wakefulness (magenta), NREM (cyan), and REM sleep (orange). (G) Pie charts showing the state with highest activity. The symbol "=" such as W=N indicates that there is no significant difference in F_z between the two states. "Unclassified" means neurons with no significant difference in F_z between sleep/wake states. (H) Pie charts showing the activity profiles in Wake-highest (left), in NREM-highest (middle), and in REM-highest activity neurons (right). (G and H) Top and bottom pie charts represent data from excitatory and inhibitory neurons, respectively. (I) Box plots indicate F_z values of Wake-highest neurons during wakefulness (magenta, W>N>R, W>R>N, and W>N=R), NREM-highest neurons during NREM sleep (cyan, N>W>R, N>R>W, and N>W=R), and REM-highest neurons during REM sleep (orange, R>W>N, R>N>W, and R>W=N). Left and right panels indicate data from excitatory and inhibitory neurons, respectively. * and *** indicate $p < 0.05$ and 0.0001, respectively.

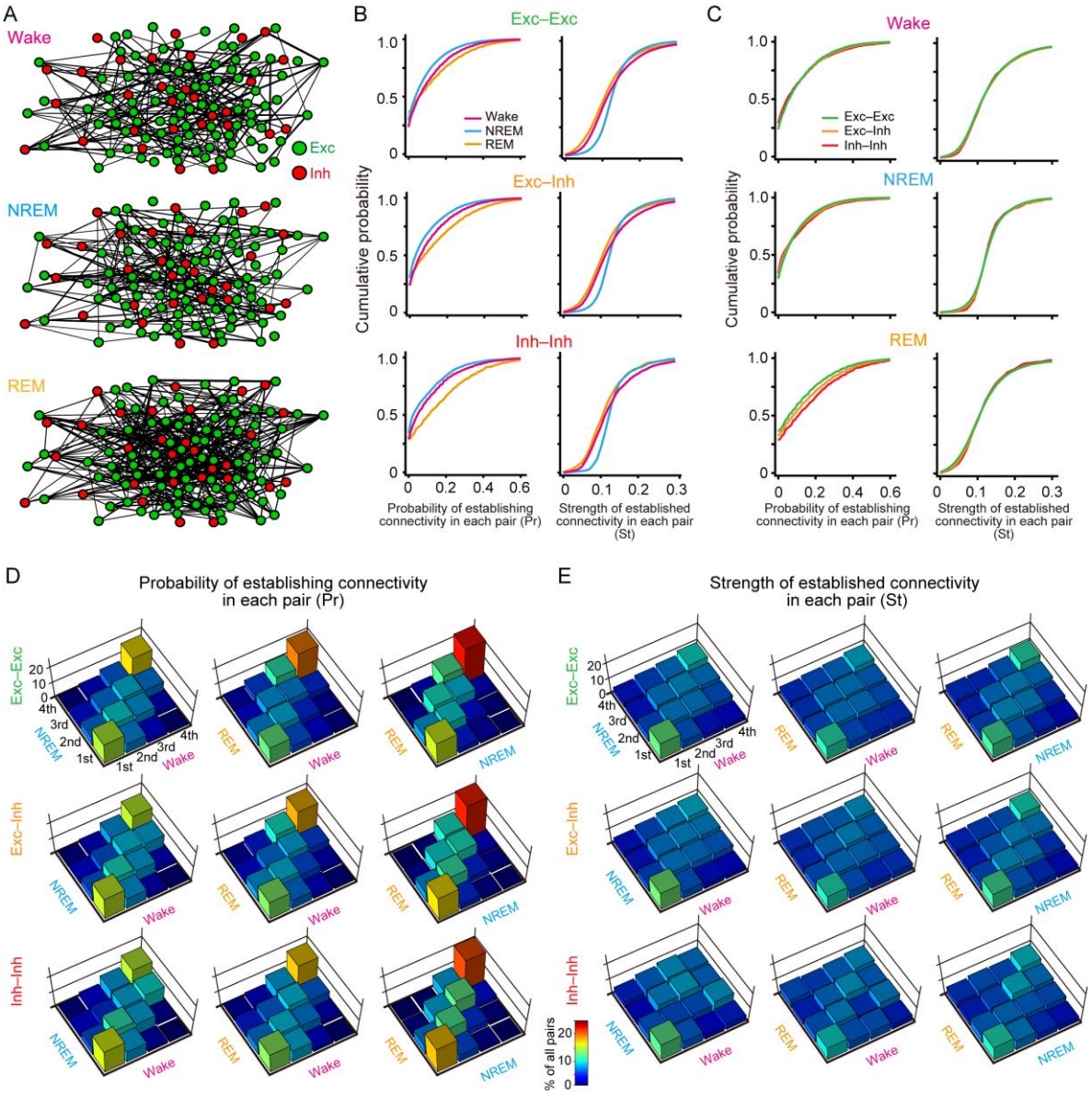

Figure 2. REM sleep increases the establishment of functional connectivity. (A) Diagrams of estimated local networks based on GGM for wakefulness (top), NREM (middle), and REM sleep (bottom). Green and red circles indicate excitatory (Exc) and inhibitory (Inh) neurons, respectively. The arrangement of points reflects the relative position of actual neurons in the two-photon image. Black lines indicate connectivity between neurons, and line thickness indicates the strength of established connectivity (St). Weak connectivity (St <0.15) is not shown. The same symbols in the network diagrams are used in the following figures. (B) (Left) Cumulative distribution of the probability of establishing connectivity (Pr) in each pair of neurons (top, Exc–Exc; middle, Exc–Inh; bottom, Inh–Inh) for wakefulness (magenta), NREM (cyan), and REM sleep (orange). (Right) Same as left panel, but for the strength of established connectivity in each pair (St). (C) (Left) Cumulative distribution of Pr during sleep/wake states (top, wakefulness; middle, NREM sleep; bottom, REM sleep) Green, orange, and red lines indicate Exc–Exc,

Exc–Inh, and Inh–Inh neuron connectivity, respectively. (Right) Same as the left panel, but for St. (D and E) Three-dimensional bar graphs showing the distribution of populations stratified into quartiles based on Pr (D) and St (E) (top, Exc–Exc; middle, Exc–Inh; bottom, Inh–Inh) for each sleep/wake state. 1st–4th indicate the top–bottom Pr or St groups.

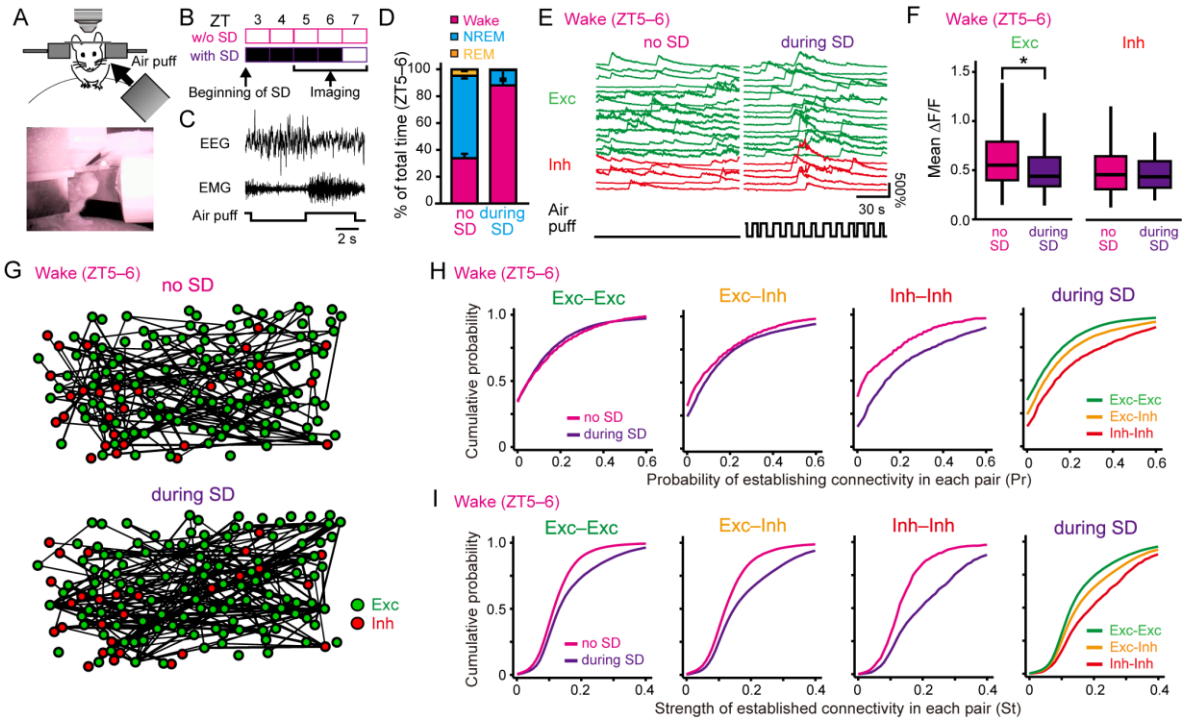

Figure 3. Functional connectivity is strengthened during sleep deprivation. (A) (Upper) A schematic diagram showing a mouse on a spherical treadmill under the objective lens during sleep deprivation. (Lower) An infrared camera image depicting a mouse of the upper panel. The white tube in front of the mouse is an air outlet. (B) Sleep deprivation and imaging schedule. Air puffs were randomly delivered every 3-7 s continuously for ZT3–6 to induce sleep deprivation (with SD, purple). Calcium imaging was performed for ZT5–7 including 1 h after cessation of the air puff delivery. (C) Representative EEG and EMG signals when the air puff was on and off (bottom line). (D) Bar graphs showing the time occupancy of sleep/wake states in ZT5–6. No SD indicates data from experiments without air puff delivery. (E) Representative relative fluorescence intensity $(\Delta F/F)t$ of GCaMP6s during wakefulness with (right, during SD) or without (left, no SD) SD. Green and red traces indicate $\Delta F/F$ of excitatory and inhibitory neurons, respectively. Bottom black lines denote air puff on and off. (F) Box-and-whisker plots showing mean $(\Delta F/F)_t$ of excitatory (Exc, left) and inhibitory (Inh, right) neurons during wakefulness during ZT5–6. The purple and magenta indicate data from experiments with SD (during SD) and without SD (no SD), respectively. * denote $p < 0.05$, Wilcoxon signed-rank test. (G) Diagrams of estimated local networks for wakefulness without SD (top, no SD) and with SD (bottom, during SD). Symbols are the same as in Figure 2A. There was a slight drift in the location of some cells due to the difference in the experiment day. (H) Cumulative distribution of Pr (first from left, Exc–Exc; second, Exc–Inh; third, Inh–Inh; fourth, overlay plots of three date on the left to compare the cell-type specificity) for wakefulness in ZT5–6. (I) Same as (H), but for St.

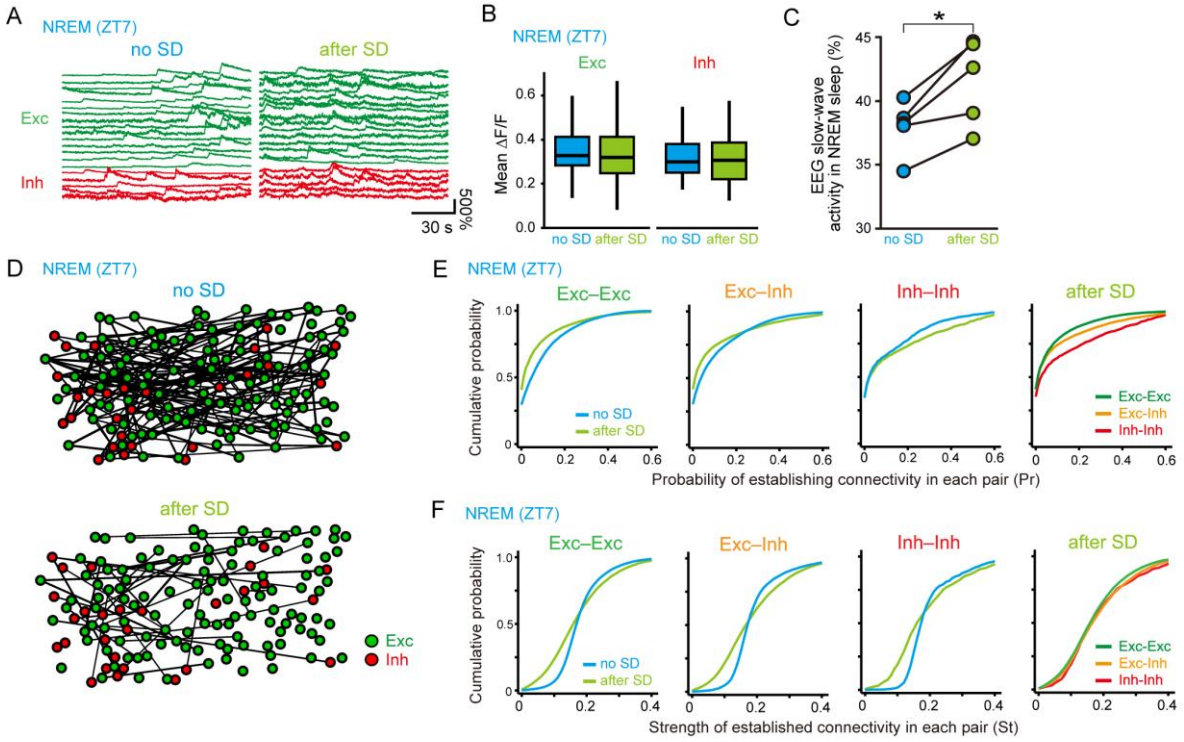

Figure 4. Functional connectivity is weakened during recovery sleep following sleep deprivation. (A) Representative relative fluorescence intensity (ΔF/F)t of GCaMP6s during NREM sleep following SD (right, after SD) or without (left, no SD) SD. Green and red traces indicate ΔF/F of excitatory and inhibitory neurons, respectively. (B) The box-and-whisker plots showing mean $(\Delta F/F)_t$ of excitatory (Exc, left) and inhibitory (Inh, right) neurons during NREM sleep in ZT7. The light green and light blue indicate data from experiments with (after SD) and without SD (no SD), respectively. (C) Percentage of slow-wave activity (2–4 Hz) in EEG (1–30 Hz). The light green and light blue indicate data from experiments with (after SD) and without SD (no SD), respectively. Data from same mice were connected straight lines. * denotes $p<0.05$. (D) Diagrams of estimated local networks using GGM for NREM sleep without SD (top, no SD) and with SD (bottom, after SD). Green and red circles indicate excitatory (Exc) and inhibitory (Inh) neurons, respectively. Symbols are the same as in Figure 2A. (E) Cumulative distribution of Pr (first from left, Exc–Exc; second, Exc–Inh; third, Inh–Inh; fourth, overlay plots of three data on the left to compare the cell-type specificity) for NREM sleep in ZT7. (F) Same as (E) but for St.

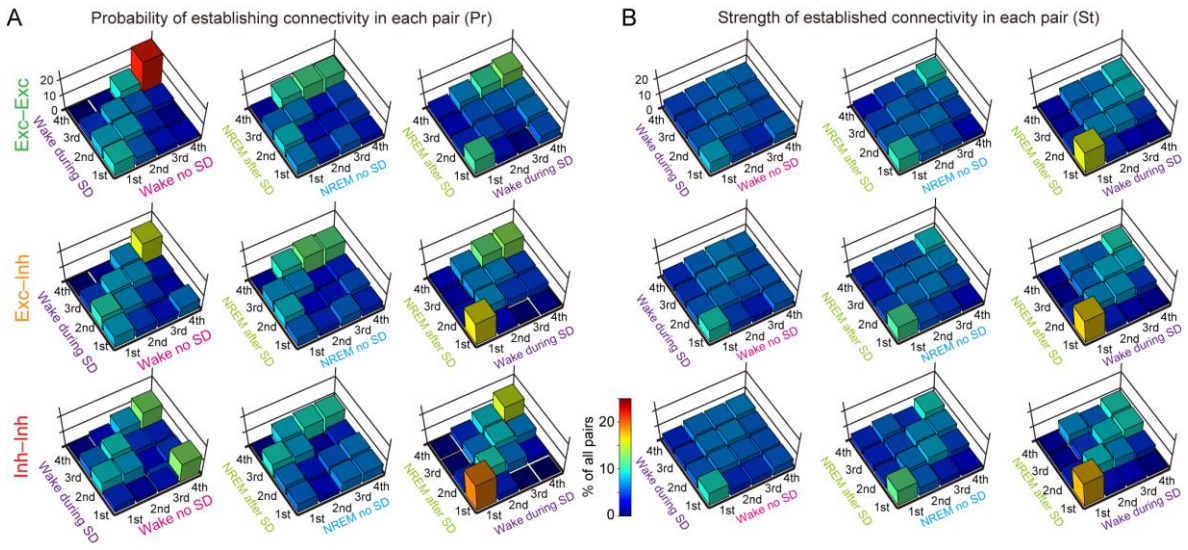

Figure 5. Dynamics of the connectivity between each neuron pair associated with homeostatic control of sleep. (A) Three-dimensional bar graphs showing the distribution of populations stratified into quartiles on the basis of Pr (top, Exc–Exc; middle, Exc–Inh; bottom, Inh–Inh) for each sleep/wake state. Wake and NREM indicates wakefulness in ZT5–6 and NREM sleep in ZT7, respectively. 1st–4th indicate the top–bottom Pr groups. (B) Same as (A), but for St.

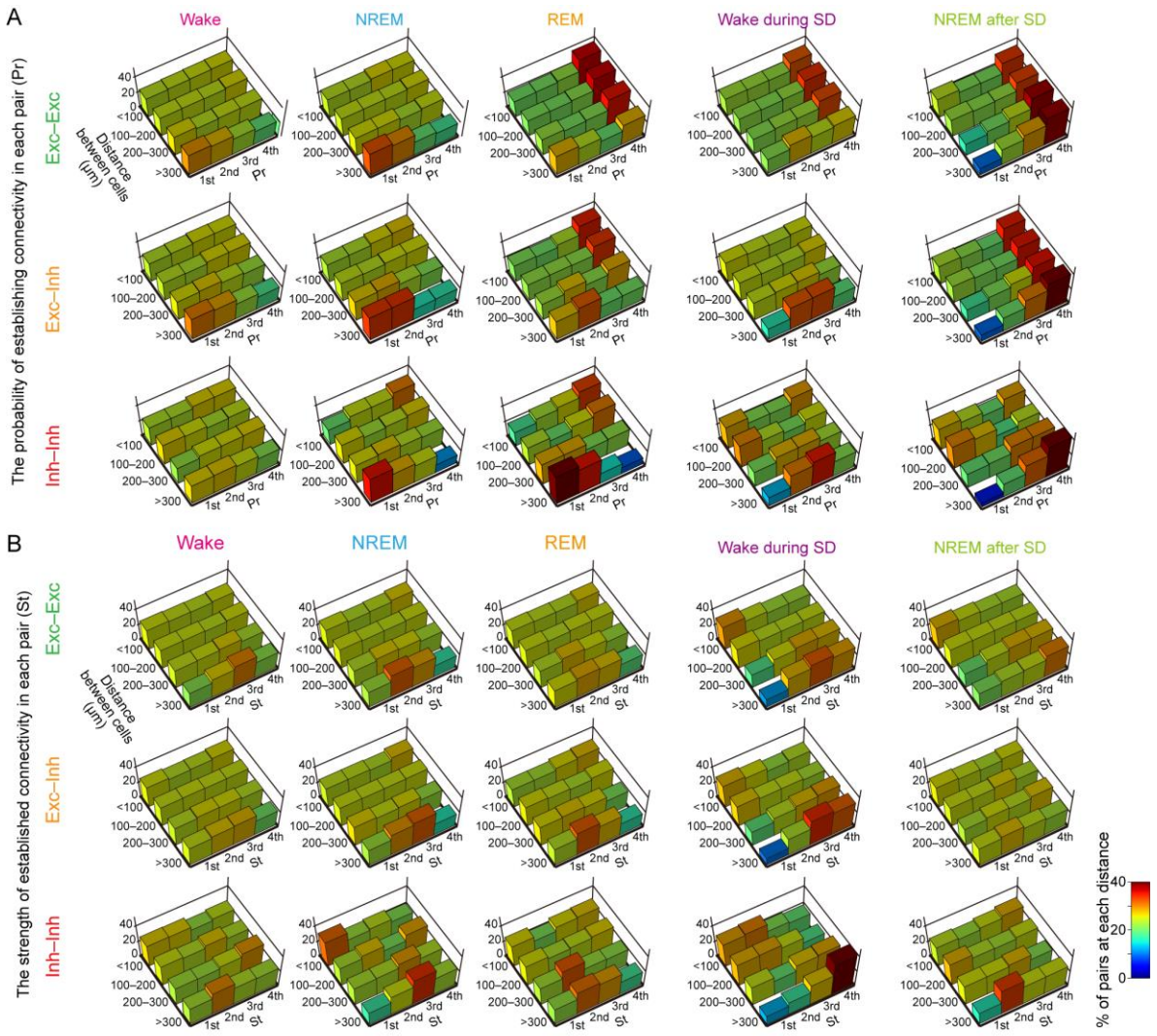

Figure 6. REM Sleep increases inhibitory connectivity with non-adjacent neurons. (A) Three-dimensional bar graphs showing the distribution of populations stratified into quartiles based on the distance between neurons and Pr (top, Exc–Exc; middle, Exc–Inh; bottom, Inh–Inh) in each sleep/wake state. 1st–4th indicate the top–bottom Pr groups). (B) Same as (A), but for St. 1st–4th indicate the top–bottom St groups.

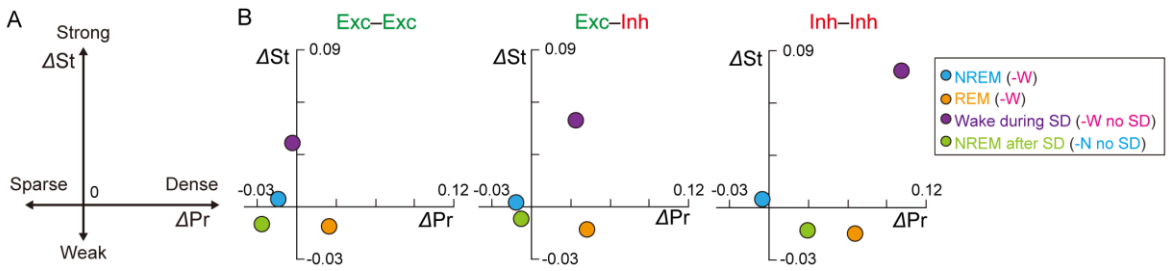

Figure 7. Dynamics of local cortical connectivity. (A) Diagram of the relationship between parameter and axis direction. (ΔPr in a state) = (mean Pr in a state) - (mean Pr in the control state). Thus, positive and negative values of ΔPr in a state indicate dense and sparse connectivity in the state, respectively. (ΔSt in a state) = (mean St in a state) - (mean St in the control state). Therefore, positive and negative values of ΔSt in a state indicate strong and weak connectivity in the state, respectively. (B) The relationship between ΔPr and ΔSt (left, Exc–Exc; center, Exc–Inh; right, Inh–Inh). The control state of NREM and REM is Wake for ZT3-7. The control states of Wake during SD and NREM after SD are Wake for ZT5-6 and NREM for ZT7, respectively. Note that Fig 7 does not fully reflect the difference in the distribution (e.g., Fig 4E) because it shows the differences in mean values.

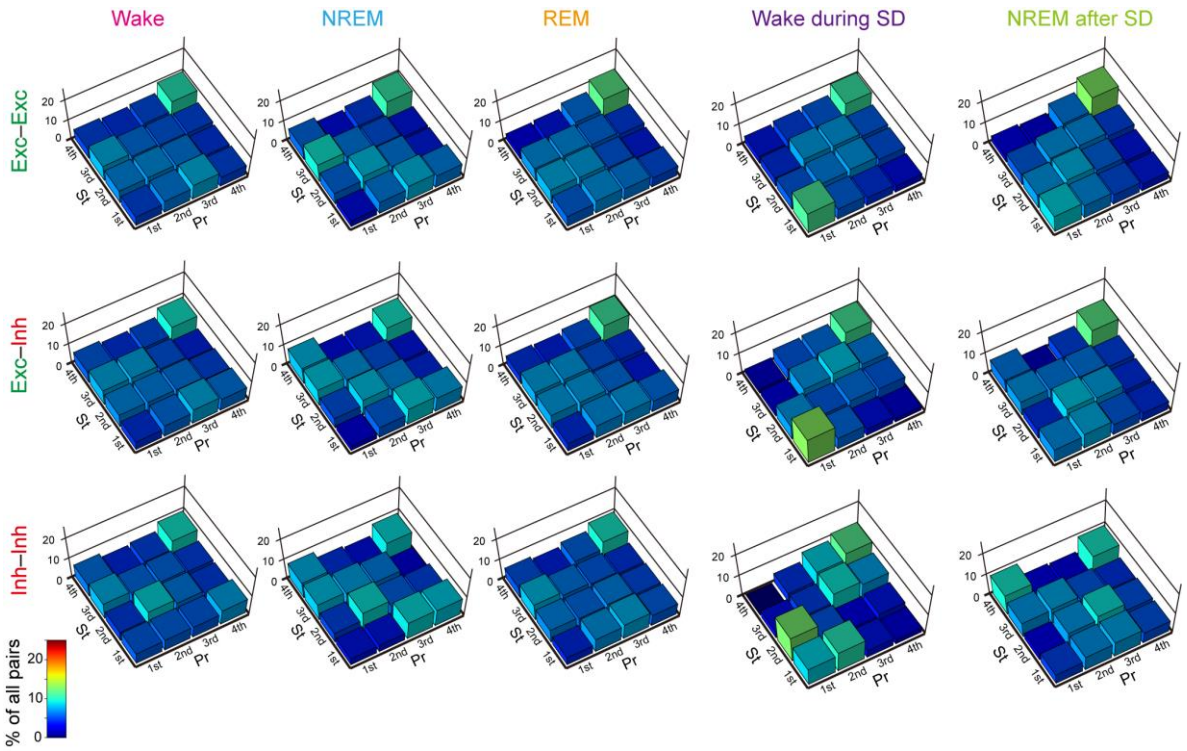

Figure S1. Relationship between Pr and St across the sleep/wake states. Three-dimensional bar graphs showing the distribution of populations stratified into quartiles based on Pr and St (top, Exc–Exc; middle, Exc–Inh; bottom, Inh–Inh) for wakefulness (first from left), NREM (second), REM sleep (third), wakefulness during SD (fourth), and NREM sleep after SD (fifth). 1st–4th indicate the top–bottom Pr groups.